The Astrophysical Journal, 779:143 (12pp), 2013 December 20 doi:10.1088/0004-637X/779/2/143

SPECTRAL SIGNATURES OF PENUMBRAL TRANSIENTS

K. Reardon[1,2,3], A. Tritschler[3], and Y. Katsukawa[4]
[1] INAF–Osservatorio Astrofisico di Arcetri, I-50125 Firenze, Italy
[2] Astrophysics Research Centre, Queen's University Belfast, BT7 1NN, Northern Ireland, UK
[3] National Solar Observatory/Sacramento Peak, P.O. Box 62, Sunspot, NM 88349, USA
[4] National Astronomical Observatory of Japan, 2-21-1 Osawa, Mitaka, Tokyo 181-8588, Japan
Received 2012 August 19; accepted 2013 October 31; published 2013 December 3

ABSTRACT

In this work we investigate the properties of penumbral transients observed in the upper photospheric and chromospheric region above a sunspot penumbra using two-dimensional spectroscopic observations of the Ca II 854.21 nm line with a 5 s cadence. In our 30 minutes of observations, we identify several penumbral-micro jets (PMJs) with cotemporal observations from Dunn Solar Telescope/IBIS and *Hinode*/SOT. We find that the line profiles of these PMJ events show emission in the two wings of the line ($\pm$0.05 nm), but little modification of the line core. These are reminiscent of the line profiles of Ellerman bombs observed in plage and network regions. Furthermore, we find evidence that some PMJ events have a precursor phase starting 1 minute prior to the main brightening that might indicate initial heating of the plasma prior to an acoustic or bow shock event. With the IBIS data, we also find several other types of transient brightenings with timescales of less than 1 minute that are not clearly seen in the *Hinode*/SOT data. The spectral profiles and other characteristics of these events are significantly different from those of PMJs. The different appearances of all these transients are an indicator of the general complexity of the chromospheric magnetic field and underscore the highly dynamic behavior above sunspots. It also highlights the care that is needed in interpreting broadband filter images of chromospheric lines, which may conceal very different spectral profiles, and the underlying physical mechanisms at work.

Key words: Sun: atmosphere – Sun: chromosphere – Sun: magnetic fields – Sun: photosphere – sunspots – techniques: imaging spectroscopy

Online-only material: color figures

1. INTRODUCTION

The chromosphere above sunspots displays an impressive variety of dynamic phenomena. Most of these are oscillatory in nature, such as umbral oscillations (Giovanelli 1972; Kneer et al. 1981; Christopoulou et al. 2000, 2001; Centeno et al. 2005), umbral flashes (Beckers & Tallant 1969; Socas-Navarro et al. 2000, 2009; Rouppe van der Voort et al. 2003), and running penumbral waves (Zirin & Stein 1972; Christopoulou et al. 2000, 2001; Bloomfield et al. 2007). For a review on the topic see Bogdan & Judge (2006). These transients exhibit changes of their spectral (and spectropolarimetric) signal on temporal (<1 minute) and spatial scales ($\ll$1 arcsec) that are still challenging to resolve concurrently (Alissandrakis et al. 1992). This challenge also holds for the rather aperiodic transients like the chromospheric inverse Evershed flow (e.g., Maltby 1975; Georgakilas et al. 2003) and of course occasional but unpredictable flaring events.

In addition to these well-established phenomena, observations with the Solar Optical Telescope (SOT; Tsuneta et al. 2008) aboard the *Hinode* satellite (Kosugi et al. 2007) revealed the presence of a novel ubiquitous activity above sunspot penumbrae that appears to be clearly discernible in running difference images of SOT Ca II H filtergrams. These penumbral transients are observed on small spatial scales (width of ~400 km, length 1000–4000 km) as jet-like brightenings of short duration (<1 minute) and were named penumbral microjets (PMJs; see Katsukawa et al. 2007). The PMJ brightness is enhanced by 10%–20% when compared with adjacent penumbral structures encompassing a sudden brightening (rise velocity >100 km s^{-1}) and gradual darkening phase.

Furthermore, it appears that PMJs are predominantly identified next to photospheric penumbral grains with their location drifting toward the umbra. The orientation of the transients with respect to the general orientation of adjacent penumbral filaments shows a center-to-limb variation: outside disk center the transients are detectable directly in the SOT Ca II H intensity and appear at an angle with respect to the general orientation of the photospheric penumbral filaments. At disk center PMJs are detectable only in the Ca II H running-difference images and appear to be aligned with the general orientation of the photospheric penumbral filaments. The variation of the inclination has been addressed by Jurčák & Katsukawa (2008). Those authors find a radial dependence of the PMJ inclination that increases from the inner to the outer penumbra. The authors suggest that PMJs are guided by the expansion of the magnetic field with height, which could explain the center-limb variation of the inclination and its radial variation across the penumbra.

Katsukawa et al. (2007) suggested that PMJs are the signature of reconnection between differently inclined field lines in the sunspot penumbra. Katsukawa & Jurčák (2010) and Jurčák & Katsukawa (2010) also found for some PMJs a corresponding blueshift in photospheric spectral lines. This suggests again magnetic reconnection as the source of some PMJs, with the observed brightenings in the Ca II H images an indication of heated plasma that is either moving supersonically or in the process of cooling down from higher temperatures. Sakai & Smith (2008) used a two–fluid model to show how a strong flow can trigger and strengthen this magnetic reconnection. Ryutova et al. (2008) suggest instead that the material is accelerated by magnetic tension and buoyancy forces, eventually reaching supersonic velocities and producing bow shocks.

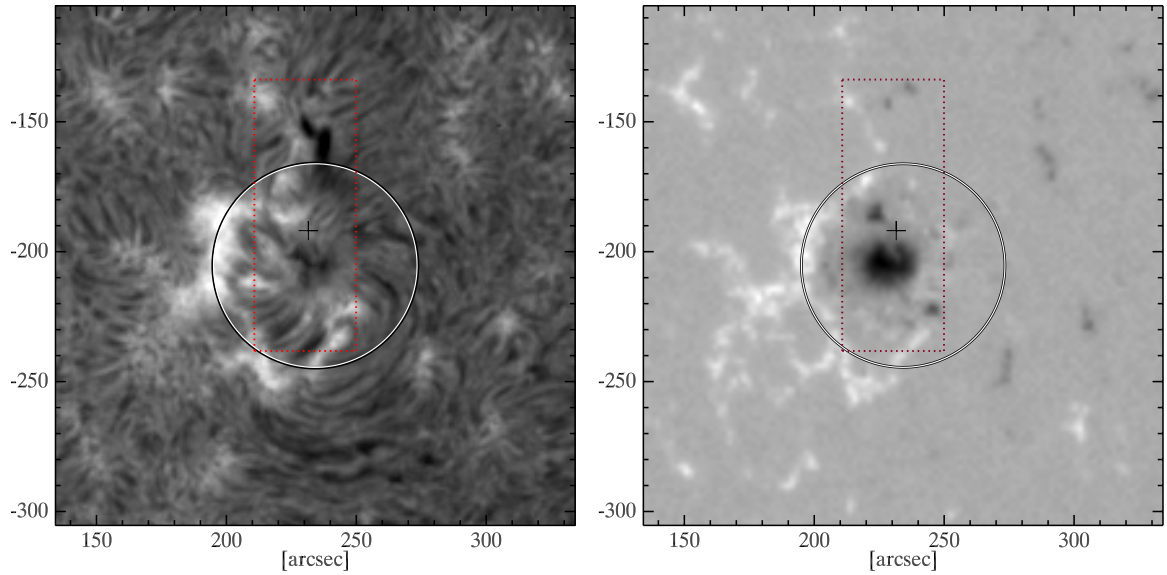

Figure 1. Left: Hα line-center image obtained with the ISOON patrol telescope at 15:13 UT, showing the full FOV of IBIS (solid circle) and of the SOT/BFI (red, dotted box). Right: *SOHO*/MDI line-of-sight magnetic field obtained at 16:03 UT. North is up, and coordinates are heliocentric distances in arcseconds.
(A color version of this figure is available in the online journal.)

The observations of PMJs in the SOT Ca II H filter have the drawback that they cannot provide any information on line-of-sight velocities. Also, due to the mixture of many atmospheric contributions within the filter passband (Reardon et al. 2009), it is not possible to independently determine the approximate height at which the PMJ signature is formed, whether in the chromosphere or in deeper, photospheric layers. Because the densities and magnetic field configuration vary greatly with height, a better understanding of the formation region of PMJs is important to understanding their nature and energy input to the upper atmosphere.

In this work we provide complementary high spatial and high spectral resolution observations that we consider imperative to further characterize (and ultimately understand) penumbral activity. Based on a sequence of high-cadence two-dimensional spectroscopic observations of the Ca II 854.21 nm line, we are able to scrutinize spectral properties and add new information about the transients such as temporal evolution and an estimate of formation height.

2. OBSERVATION DESCRIPTION

Observations were carried out on 2007 August 28 at the Dunn Solar Telescope (DST) of the National Solar Observatory (NSO)[5] using the dual Fabry-Perot Interferometric Bidimensional Spectrometer (IBIS; Cavallini 2006). Real-time seeing correction and image stabilization during the observations were accomplished by the high-order adaptive optics system installed at the DST (Rimmele 2004).

We observed the moderately sized, leading sunspot of active region NOAA 10969, located at S05, W14. Figure 1 shows the general appearance of the region in Hα as observed by the ISOON (or OSPAN) patrol telescope (Neidig et al. 1998) and the magnetic field measured by *SOHO*/MDI (Scherrer et al. 1995). The active region was in a stable to decaying phase of its evolution, with the MDI observations obtained in the 2 day interval surrounding our data showing some evidence of magnetic field dispersal through moving magnetic features (MMFs). Previous work has shown a correlation between MMFs and both Ellerman bombs (Georgoulis et al. 2002) and Hα surges and X-ray jets (Canfield et al. 1996).

In the 28 minute interval from 15:09:23 to 15:37:50 UT we obtained 298 scans of the Ca II 854.2 nm line. The line was sampled on a coarse grid of 14 non-equidistant wavelength points covering a total range of 0.25 nm and with a step size around the line core of 15 pm. The FWHM of the IBIS instrumental profile at 854 nm is 4.4 pm (Reardon & Cavallini 2008). The entire spectral line scan was acquired within 5.3 s, with the central 0.1 nm of the line being acquired in less than 3 s. The spectral channel data were obtained at full resolution with $0\farcs082$ pixel^{-1} and a total field of view (FOV) of $80''$ in diameter.

Together with each image in the narrowband channel, an image was obtained in the broadband channel of IBIS using an interference filter centered at 721 nm with an FWHM of 10 nm. Strict simultaneity was ensured through the use of a common shutter for both channels. The broadband images were used to generate a sequence of 60 speckle reconstructions with a cadence of 27 s.

We applied standard calibration procedures for IBIS, including dark, gain, and blueshift correction (for details, e.g., Cauzzi et al. 2008). The line-center reference wavelength position was determined from the mostly quiet Sun region surrounding the sunspot in the full observed field. Grid targets were used for alignment purposes to determine the actual rotation and image scale differences between the spectral images and the simultaneous broadband images, using the narrowband data as a reference. The broadband data were employed to correct for transparency fluctuations, rigid image shifts, and an initial correction of the seeing-induced image distortions (destretch). As a reference for the destretch algorithm we compute speckle reconstructions based on the broadband images using the speckle masking code developed by Wöger & von der Lühe (2007). Because of the significant wavelength offset between the broadband and

[5] Operated by the Association of Universities for Research in Astronomy (AURA), Inc., for the National Science Foundation.

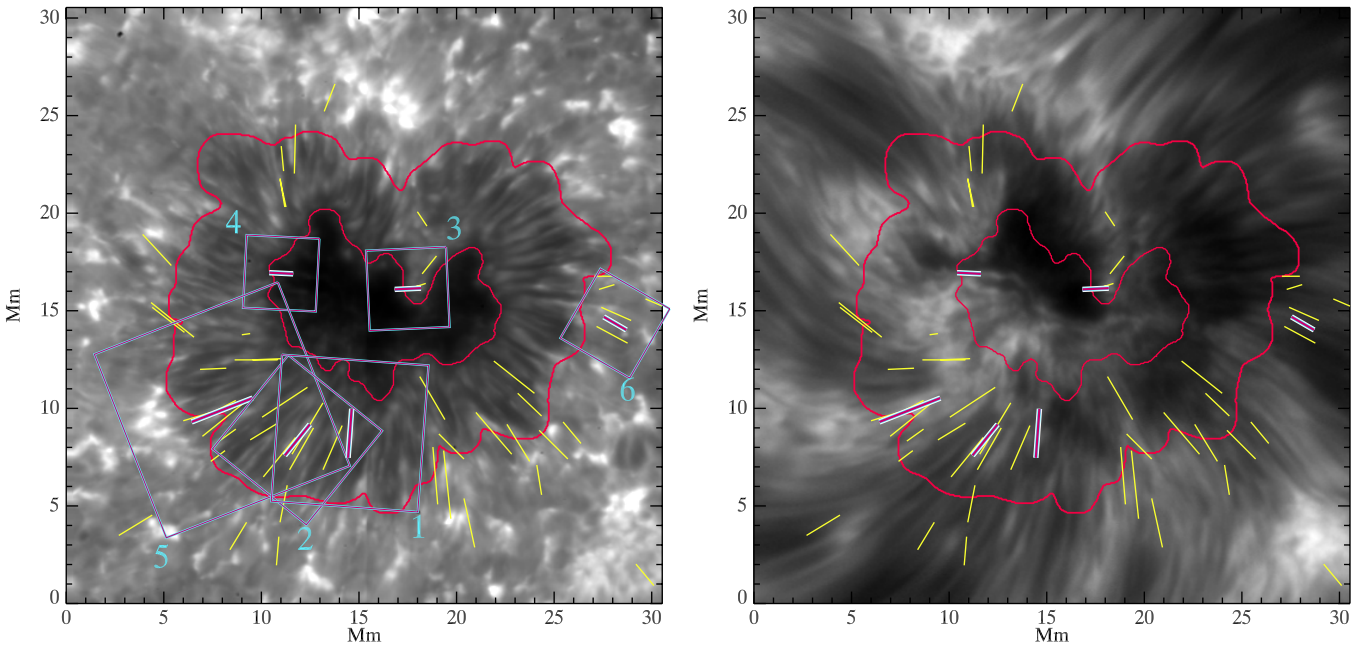

Figure 2. Left: Ca II H filtergram obtained with the SOT/BFI. Right: Ca II 854.21 nm line-core image obtained with IBIS. Red contours indicate boundaries of umbra and penumbra. The yellow lines indicate the location, orientation, and approximate length of the identified penumbral transients. We have selected six different events that characterize a variety of these behaviors to examine in further detail. These events are identified by the red lines, with the blue boxes in the left figure defining the areas displayed in Figures 3, 6, 8, 10 and 12.

(A color version of this figure is available in the online journal.)

spectral data, it was necessary to perform a secondary destretching on the sequences of monochromatic images at each of the 14 sampled wavelengths.

We compare the IBIS observations with co-temporal Ca II H filtergrams obtained with the broadband filter instrument (BFI) part of the focal plane package of the SOT aboard *Hinode*. The Ca II H filtergrams are part of a ∼7 hr sequence taken from 10:08:27 to 16:59:4 UT on 2007 August 28. The FOV of the Ca II H filtergrams is 42″ × 112″ with a detector scale of about 0.″11 pixel^{-1}.

2.1. Event Identification

We manually examined the sequences of images taken with IBIS in the nominal core position and the blue and red wing ($\delta\lambda = 0.0, \pm 0.04$ nm, respectively) of the Ca II 854.2 nm line. The line core originates from layers nominally at ∼800–1000 km (Cauzzi et al. 2008), and any brightening detectable at this wavelength is therefore of chromospheric origin. The wing wavelengths, on the other hand, correspond to the so-called knee of the Ca II 854.2 nm line formed in much lower layers at about 500 km (Cauzzi et al. 2008).

For this examination we used both the calibrated intensity images and sequences of running difference images. Using a 42″ × 42″ subfield centered on the sunspot, we studied the penumbra and the immediate surrounding areas in order to identify small-scale rapid transient brightenings that occurred in any of these three wavelengths. A small flare occurred over the northeastern portion of the penumbra and umbra, but was not included in this study. We recorded for each event the time of peak intensity, as well as the two points that defined the maximum extent and orientation of the event. We identified 55 events that showed a rapid increase and decrease in intensity, with many events lasting 30 s or less. Many of these events have a co-spatial signature in the corresponding SOT Ca II H filtergrams. Some of these events would have been identified as PMJs from the SOT data using the same algorithm applied by Katsukawa et al. (2007). Others are too weak to be automatically identified in the SOT data, even with the additional "noise" caused by residual seeing distortions in the running difference IBIS images.

These events are shown in Figure 2, with the line between the endpoints plotted over both an example SOT Ca II H image and an IBIS image taken in the core of the Ca II 854.2 nm line. The median spatial extent of the events was 2.″3 or 1.6 Mm. Given the limited duration of the observations (∼30 minutes) and the use of manual identification techniques, we are hesitant to make any broad statistical conclusions about the number or distribution of events. However, with the four-dimensional data set, we are able to examine the spectral and spatial variations that occur in each event in detail.

3. RESULTS

The most striking result is that these transients, identified as rapid brightenings in sequences of monochromatic images, actually encompass a range of spectral behaviors, indicating that there are actually multiple physical processes that can produce the observed penumbral transients. Some of the observed spectral signatures are reminiscent of other well-known phenomena typically observed in locations other than sunspot penumbrae. We have selected six events that characterize a variety of these behaviors, and whose locations are indicated by the red lines and blue boxes in Figure 2.

In order to visualize the temporal, spatial, and spectral evolution of these events, we show different slices through the (x, y, λ, t) data cube. In Figures 3, 6, 8, 10, and 12, we show images at five different wavelengths at the peak time of each of the selected events. These images, with FOV and orientation indicated by the corresponding blue boxes in Figure 2, are shown both as the original snapshot (upper row) and as the snapshot

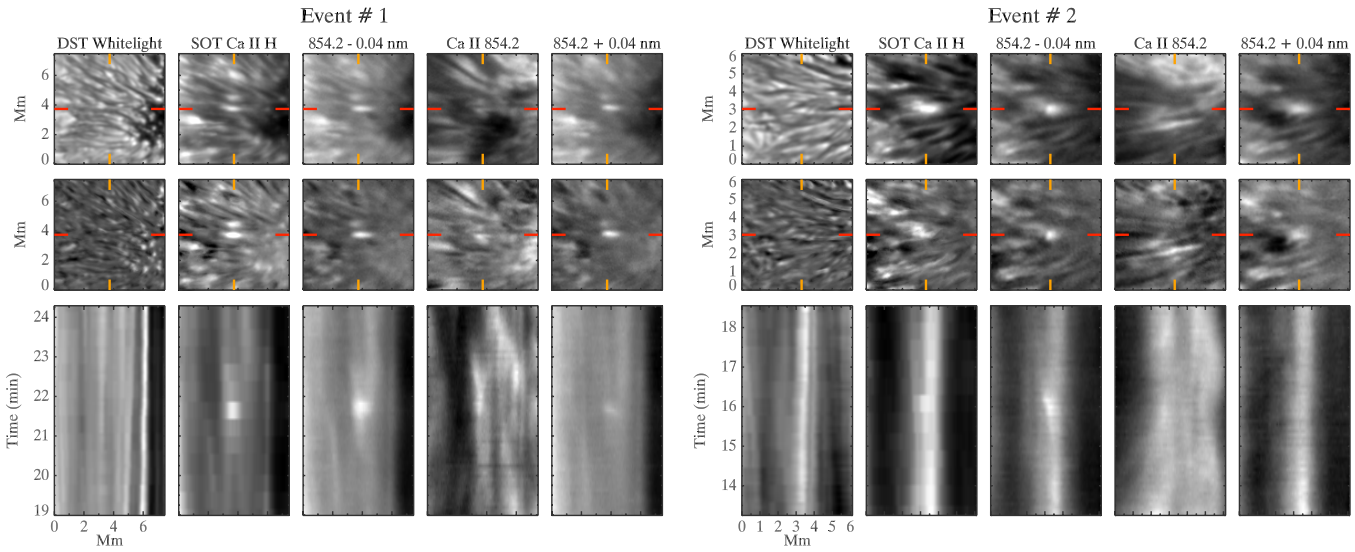

Figure 3. Spatio-temporal behavior of Event #1 (left) and #2 (right). Upper panel, left to right: images at five different wavelengths (whitelight DST, SOT Ca II H, blue line wing, line core, and red line wing of the IBIS Ca II 854.21 nm line) at the peak time of the event. The event location is indicated by the intersection point of the red and orange tickmarks. The zoomed areas are as indicated in Figure 2 and oriented such that the umbra is located to the right of the displayed images. Middle panel: same as upper panel but median over the whole time sequence subtracted. Bottom panel: $(x - t)$ slices showing the temporal evolution of the cut indicated by the red tickmarks in the images of the upper panel.

(A color version of this figure is available in the online journal.)

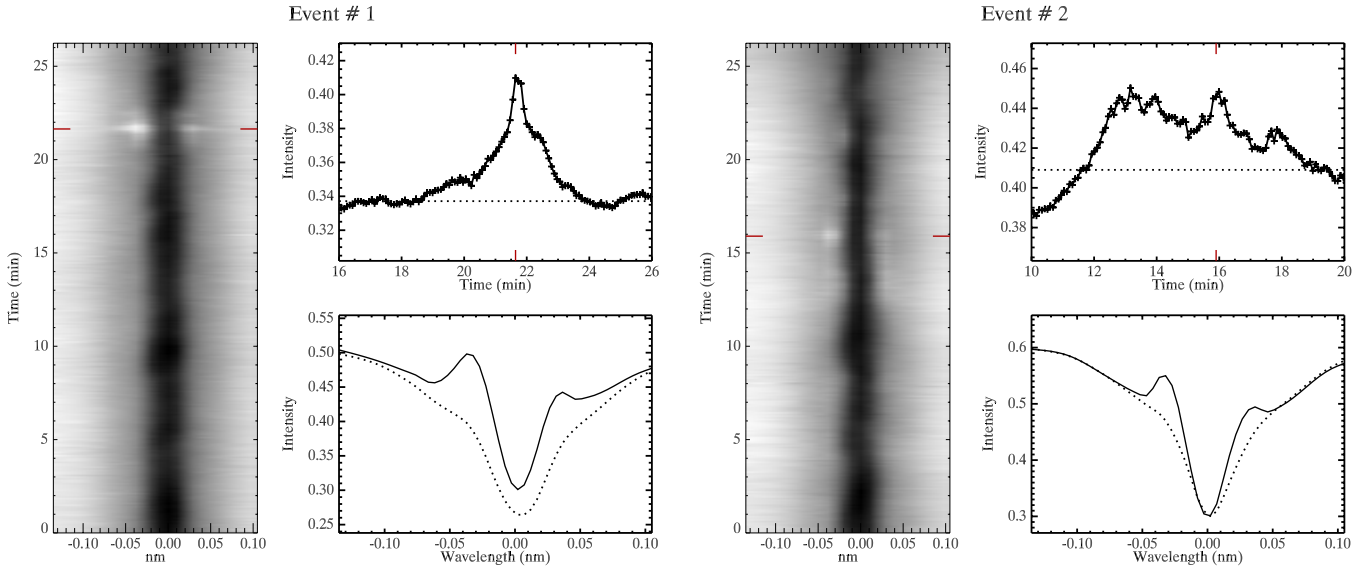

Figure 4. Spectral-temporal behavior of Event #1 (left) and #2 (right). Left: temporal evolution in Ca II 854.2 taken at the intersection of the red and orange tickmarks (event location) in the corresponding snapshot images in Figure 3 (upper panel). Red horizontal tickmarks mark the peak time. Top right: light curve at the event location calculated by averaging over the central wavelengths (±0.06 nm) of the Ca II 854.21 nm line. The dotted line indicates the average intensity over the full time sequence. Bottom right: observed spectrum at peak time (solid) and event location compared to the spectrum at the event location when averaged over the whole observing period (dotted).

(A color version of this figure is available in the online journal.)

after subtracting the median image for the whole time series (middle row) for each of the relative wavelength bands. Below the images, $(x - t)$ slices are displayed showing the temporal evolution of the cut through the image indicated by the red tickmarks in the images (bottom row). The slices cover a 5 minute period centered on the peak time of the event.

Figures 4, 7, 9, 11, and 13 instead show the spectral evolution (left), the light curve (top right), and the observed spectrum at peak time (bottom right) of the corresponding event. The spectral evolution is extracted at the event location defined by the intersection of the red and orange tickmarks in the corresponding snapshots. The light curve is taken at this same point averaged over the inner portion (±0.06 nm) of the spectral line profile, with the dotted line indicating the average intensity over the full time sequence. The observed spectrum is taken at the time of the event maximum (indicated by the red tickmarks in the spectral slices) and is compared to the profile (dotted) at the event location averaged over the duration of the observations.

In the following sections, we will examine the selected events in detail.

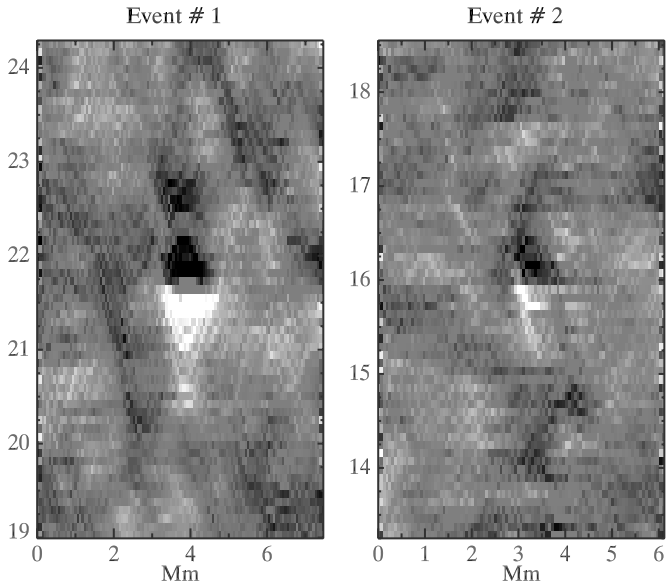

Figure 5. $x-t$ plot of the running difference of the blue-wing intensity along the length of Events #1 and #2 around the time of the peak intensity for each event. The spreading brightening beginning 1 minute prior to the peak intensity is visible to different degrees in both events.

3.1. Event Class 1: Ellerman Bombs

The most significant penumbral event in our ∼30 minute time sequence occurred in the southern part of the penumbra on the opposite side of the spot from disk center and is identified in Figure 2 as Event #1. This transient, shown in detail in Figure 3 (left), was easily seen in both SOT and IBIS data as a rapid, elongated brightening that evolves parallel to the orientation of the underlying penumbral filaments, reaching a full length of approximately 1.5 Mm. Because the filaments at this location are roughly radial with respect to disk center, this orientation is to be expected.

Other similar but significantly smaller transients are seen in the data. As an example, Event #2 is shown in Figure 3 (right). This event occurs in a region that shows a generally enhanced brightness for several minutes both before and after the transient. The region is brighter in the SOT Ca II H images than the IBIS Ca II 854.2 images, probably due to the increased brightness temperature response for the more blueward line. A corresponding bright background is also visible in the white-light images, perhaps indicating the presence of a magnetic element or temperature enhancement spanning a significant portion of the photosphere.

The corresponding spectra at the time of Events #1 and #2 (Figure 4, left and right, bottom right) show a strong similarity, the basis on which we have grouped them together. They show a conspicuous line-wing emission in the knee of the line around ±0.04 nm, while the line core is less affected. A similar brightening in the wings of Ca II H presumably leads to the intensity enhancement seen in the SOT filtergrams. No strong Doppler shifts are seen in the core of the Ca II 854.2 line.

Both events show a blue-red asymmetry in the sense that the enhancement in the blue wing of Ca II 854.2 nm is greater than that of the red wing. Given that the line core position and shape are not strongly modified, this may indicate the presence of a blue shifted emission component, but the simple interpretation of self-reversed line profiles can be misleading. Comparison of the observed profiles with outputs from NLTE radiative transfer calculations could provide a better way to extract information on the underlying physical conditions in the solar atmosphere, but this approach is at present highly challenging for such dynamic events.

The brightness evolution of Events #1 and #2 is also illustrated in the upper right panels of Figure 4. The light curves show that the episodes of strongest brightening last less than 1 minute, with both a rapid rise and decay phase of only about 10 s or less.

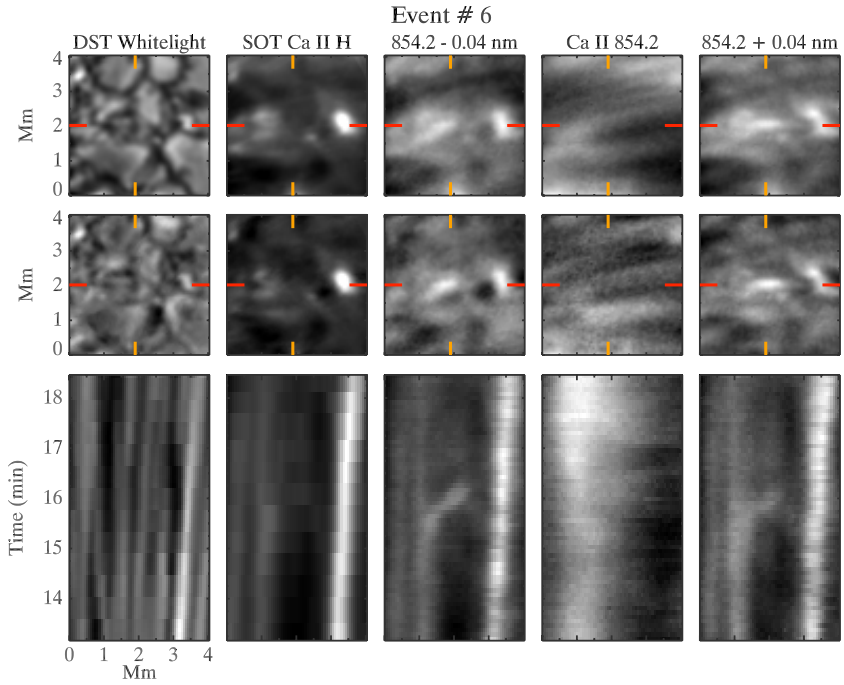

Figure 6. Spatio-temporal behavior of Event #6. Same as Figure 3.
(A color version of this figure is available in the online journal.)

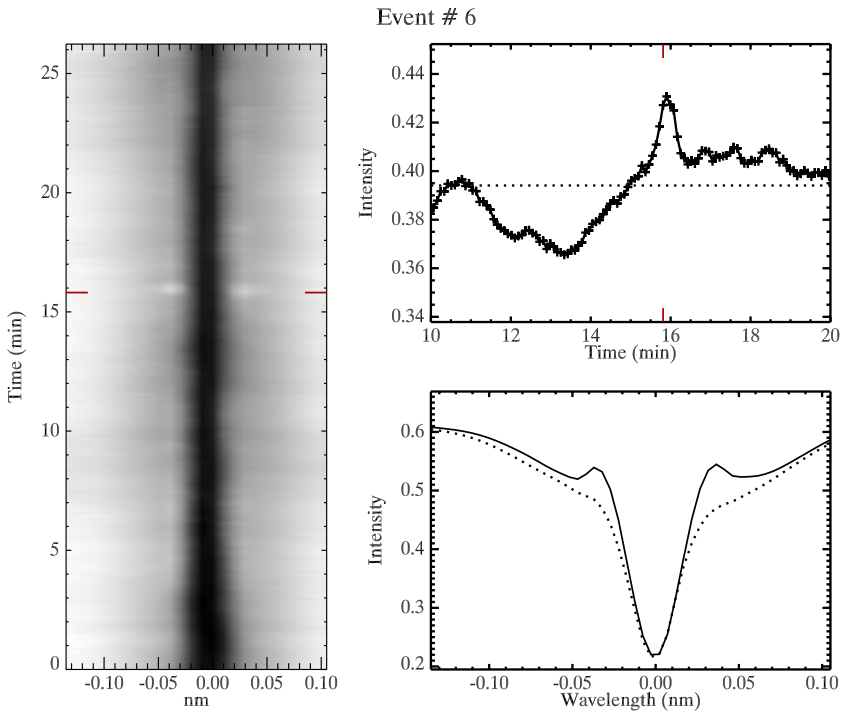

Figure 7. Spectral-temporal behavior of Event #6. Same as Figure 4.
(A color version of this figure is available in the online journal.)

In between, the intensity remains fairly constant around the peak for a brief period of around 30 s. The observed peak intensities seen in the light curves for these two events are approximately 20% and 10%, respectively, of the local, time-averaged intensity.

Especially notable in Event #1 is a gradual onset of the transient that begins up to 2 minutes before the peak intensity, as well as a slow decay that lasts almost 2 minutes afterward, as seen in the light curves. In the $(x - t)$-slice of the intensity in the blue wing of the Ca II 854.2, an elongated brightening can be already seen growing almost 1 minute before the peak brightness ($t \sim 21.0$ minutes). The evolution of the pre-event brightening can be more clearly seen by making $(x - t)$ slices from the running difference images in the blue wing Ca II 854.2, as shown in Figure 5. White indicates an increase in the intensity between successive time steps, and black a decrease. In Event #1, the main impulsive brightening is observed at 21.5 minutes, but a very small brightening occurs in this location at 20.5 minutes. A brightening is then seen to spread progressively outward from this confined onset location along the axis of the event. The expansion of this brightening front appears to be essentially constant at this resolution, reaching 1.5 Mm in 1 minute for an average growth rate of 12 km s^{-1}. Following the peak of the event, the intensity fades almost symmetrically with the growth, with the brightness enhancement receding back along the length of the event at a comparable rate. Similar behavior is seen in Event #2 (right panel of Figure 5), though due to its smaller overall enhancement the signal is noisier.

Examined in this manner, no highly supersonic apparent propagation velocities or impulsive accelerations are observed. Rather, by spectrally isolating the emission in the blue wing of Ca II 854.2, we can see that the impulsive brightening at the event peak occurs uniformly over the length of a structure that had already been "triggered" 1 minute beforehand.

These precursors may be disturbances, in density or temperature, that propagate along the field lines, until they produce a reconnection event or other destabilization of the existing field topology. These could also be the signatures of the bow shocks predicted by Ryutova et al. (2008), in which plasma along reconnected field lines is accelerated upward by magnetic tension and buoyancy until it reaches supersonic velocities. The shock would rapidly heat material along the length of the moving plasma, and the precursor could be the signature of a "slingshot" shock that runs out in front of the bow shock. Given our viewing angle, we are essentially looking down on the PMJ from above, so the curvature or spatial offset between these two shocks would not be visible.

As an interesting comparison, we also show in Figures 6 and 7 the same types of images and spectral plots for Event #6, which occurred to the west of the sunspot, outside of the penumbra (see Figure 2). The spectro-temporal behavior (Figure 7) is very similar to that of the penumbral transients, with brightenings in the blue and red wings (though more symmetric than that seen in Events #1 and #2) but no modification of the line core. The light curve and duration of the brightening are also comparable, with a short, peaked brightening lasting less than 1 minute.

The images show a bright streak in both the blue and red wings of Ca II 854.2 that appears to be only roughly aligned with the chromospheric fibrils seen in the line core. The $(x - t)$ slices show a rapid transverse motion along the direction of the elongated brightening from the beginning to the end of the event (15.5–16.5 minutes). The apparent horizontal motion of this brightening is about 20 km s^{-1}. Interestingly, no signature of this event is discernible in either the images or $(x - t)$ plots from the Ca II H filter.

This indicates that the same processes that produce penumbral transients may be at work also in other regions of the solar atmosphere, but that they might be more difficult to observe through a broadband filter. The presence of similar Ellerman-bomb-type events even outside the penumbra would be

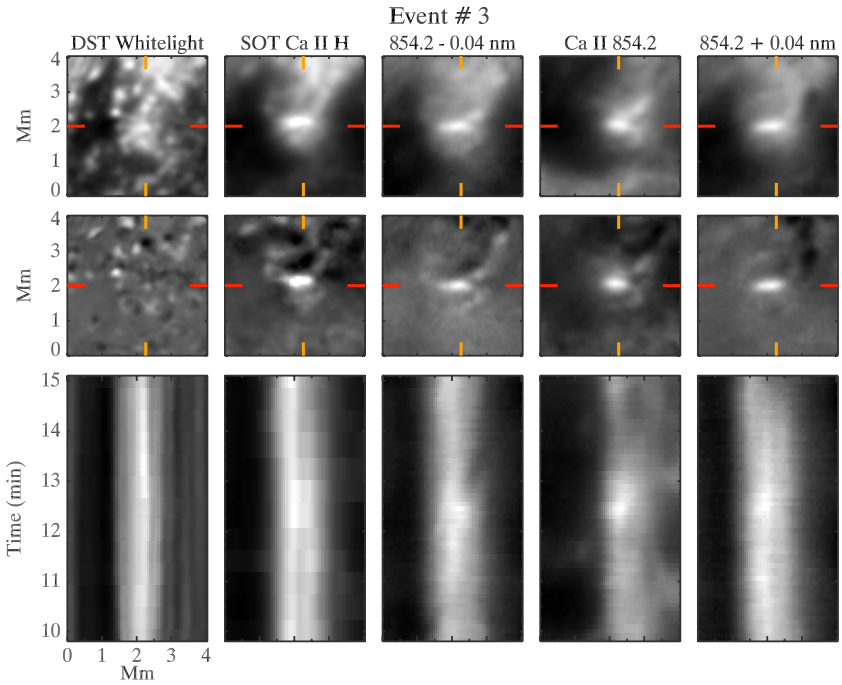

Figure 8. Spatio-temporal behavior of Event #3. Same as Figure 3.
(A color version of this figure is available in the online journal.)

consistent with the association of these PMJs with MMFs and the associated serpentine magnetic field lines (Schmieder & Pariat 2007; Archontis & Hood 2009).

The spectral signature of Events #1 and #2 is strongly reminiscent of the classical Ellerman bomb (Ellerman 1917) or *moustache* (Severny 1956) spectra. These features have long been studied in Hα (Roy & Leparskas 1973; Kurokawa et al. 1982; Denker et al. 1995; Schmieder et al. 2002; Socas-Navarro et al. 2006; Matsumoto et al. 2008; Watanabe et al. 2011), but Fang et al. (2006) and Pariat et al. (2007) have both observed Ellerman bombs simultaneously in Hα and Ca II 854.2, demonstrating the similar response in both lines. The profiles we observe in these penumbral transients correspond well to the Ellerman bomb signatures shown in Figure 2 of Fang et al. (2006).

The predominance of the enhancement near the "knees" of the chromospheric lines, with little modification of the core intensities, indicates that the physical process at work is occurring somewhere around the temperature minimum region (Cauzzi et al. 2008). Various models have been proposed to explain the Ellerman bomb spectral signatures (Kitai & Muller 1996; Schmieder et al. 2002; Georgoulis et al. 2002; Fang et al. 2006), all based on dissipation of magnetic energy around the temperature minimum region. Alternatively, the enhancement may be visible only in the line wings because overarching super-penumbral fibrils have enough opacity at the line core wavelengths that the chromospheric emission from below is obscured.

3.2. Event Class 2: Acoustic Shocks

Another type of brightening is labeled as Event #3 in Figure 2 and shown in detail in Figures 8 and 9. These events occur in a region that shows a slight discontinuity in the radial penumbral structure. In the broadband continuum images from the photosphere, this penumbral intrusion is visible if not immediately noticeable, while in the map of the magnetic flux measured from the SOT/SP several hours earlier this intrusion corresponds to a noticeable gap with greatly reduced magnetic field strength. In the chromosphere, this region also shows an apparent lack of radial super-penumbral fibrils. A series of such fibrils seem to be rooted along the edges of this intrusion, rather than into the edge of the umbra as is typical in other portions of the sunspot.

In this region, the Ca II 854.2 spectra show repeated velocity excursions characteristic of acoustic oscillations driven by the photospheric motions. Many of these events seem to show the rapid-onset blueshifts and gradual transition to large redshifts that are typical of strong acoustic shocks (Cauzzi et al. 2007; Vecchio et al. 2009) and the associated dynamic fibrils (Hansteen et al. 2006). Such behavior is typically seen in the inclined fields at the edge of magnetic network concentrations (Vecchio et al. 2007, 2009; Stangalini et al. 2011), and indeed these events seem to be more prevalent at the edge of this intrusion.

The images of Event #3 shown in Figure 8 show an elongated brightening close to the boundary of the umbra. The brightening is clearly visible in the SOT Ca II H images, as well as in the wing and core images from Ca II 854.2. Events in this region tend not to show such a pronounced elongation or the same tendency for a radial orientation as the events elsewhere in the penumbra.

In the spectral-time slices shown in Figure 9 (left), the initial phase of this event (at $t = 12.5$ minutes) shows a strong brightening across the full core of the chromospheric line. The spectra show enhancements in the two wings of the profile and also a 50% brightening of the line core. Overall the event appears to be more pronounced in all wavelengths than the Ellerman-bomb-type events. The blue asymmetry in the event line profile would also be consistent with the explosive propulsion of material upward in these acoustic events (followed several minutes later by a strong downflow of the returning material).

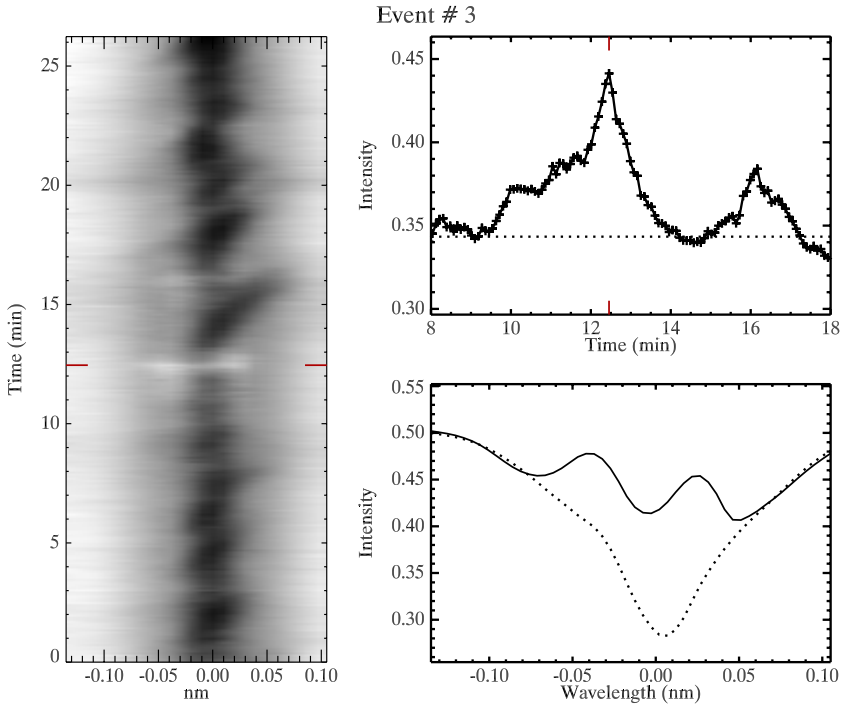

Figure 9. Spectral-temporal behavior of Event #3. Same as Figure 4.
(A color version of this figure is available in the online journal.)

The light curve shows that this event also lasts about 1 minute, with perhaps a more gradual onset and decay phase as compared to the Ellerman bomb events. The brightness increase in this event is approximately 25% above the average intensity at the peak, somewhat greater than the enhancement seen in those events (see Figure 4). Another smaller brightening seems to occur at $t = 16.0$ minutes, approximately 4 minutes after the initial event. However, such repetition does not seem to be the rule.

3.3. Event Class 3: Umbral Flash

A third type of transient is seen above the boundary between the photospheric umbra and penumbra, as illustrated by Event #4 in Figure 2. The images in Figure 10 show this region, with the umbra in the righthand portion of the images. A small brightening, confined and with no apparent elongation, is visible in all the Ca II images. The photospheric white-light image shows many penumbral grains, the bright ends of penumbral filaments, but none seem to closely correspond to the location of this event.

The $x-t$ slices of the line-core intensity (and to a lesser extent the other wavelengths) show a brightening in the umbra prior to the event that moves radially outward toward the penumbral boundary at an apparent horizontal speed of approximately 25 km s^{-1}, typical of the apparent transverse velocities of spreading umbral flashes. The $\lambda - t$ display of this event (Figure 11, left) shows a steady emission in the line core whose fluctuations are typical of umbral flashes and the 3–minute oscillations (e.g., Rouppe van der Voort et al. 2003). However, the impulsive brightness increase of Event #4 is much stronger than any of the umbral flashes at this location, and the enhancement lasts for 1.5 minutes, much longer than normal for umbral flashes. Temporally extended brightenings of this type are not seen in any of the profiles simulated by Bard & Carlsson (2010). This relatively long duration indicates that this event is not an umbral flash, but perhaps an indication of magnetic dissipation above the sunspot umbra. We also note that this region is near where a small flare was observed later in the observing sequence.

3.4. Event Class 4: Chromospheric Modification

A curious event occurs in the southeast corner of the sunspot, labeled as Event #5 in Figure 2. This event occurs above an undistinguished portion of the photospheric umbra, but in a region characterized in the Ca II 854.2 images by a "gap" in the dark superpenumbral fibrils. On the northern side of this gap the superpenumbral fibrils connect to the nearby trailing polarity, while below the gap the fibrils connect to more distant regions of opposite polarity. This change in the magnetic orientation between these two areas is also seen in the different orientations of the penumbral transients above and below Event #5 as seen in Figure 2.

The images of the Ca II 854.2 line core and red wing (+0.04 nm) in Figure 12 show two distinct footpoints, one indicated by the tick marks at $x = 6$ Mm, and the second to the left at $x = 4$ Mm. Comparison with the white-light image shows that the right footpoint lies within the penumbra proper, while the second footpoint is at the outer boundary of the penumbra. The $x-t$ slice shows that both footpoints brighten simultaneously.

The two footpoints aligned along the penumbral filaments indicate the possible presence of a magnetic bipole that has emerged into the chromosphere above the penumbra. The magnetic field of this bipole could reconnect with the pre-existing chromospheric field. The spectral profile of this event seen in Figure 13 shows core emission across the line profile, with two peaks seen in the line wings. In this case, the red wing is brighter than the blue wing. The onset of this event is very rapid, with the impulsive rise in the intensity taking place in less than 15 s. The decay in the intensity after the peak is almost equally fast.

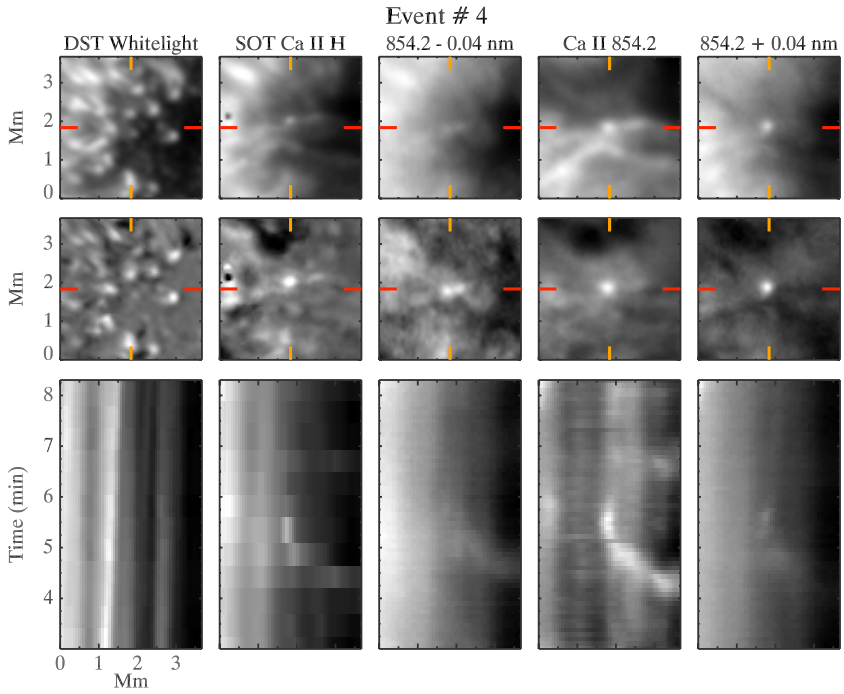

Figure 10. Spatio-temporal behavior of Event #4. Same as Figure 3.
(A color version of this figure is available in the online journal.)

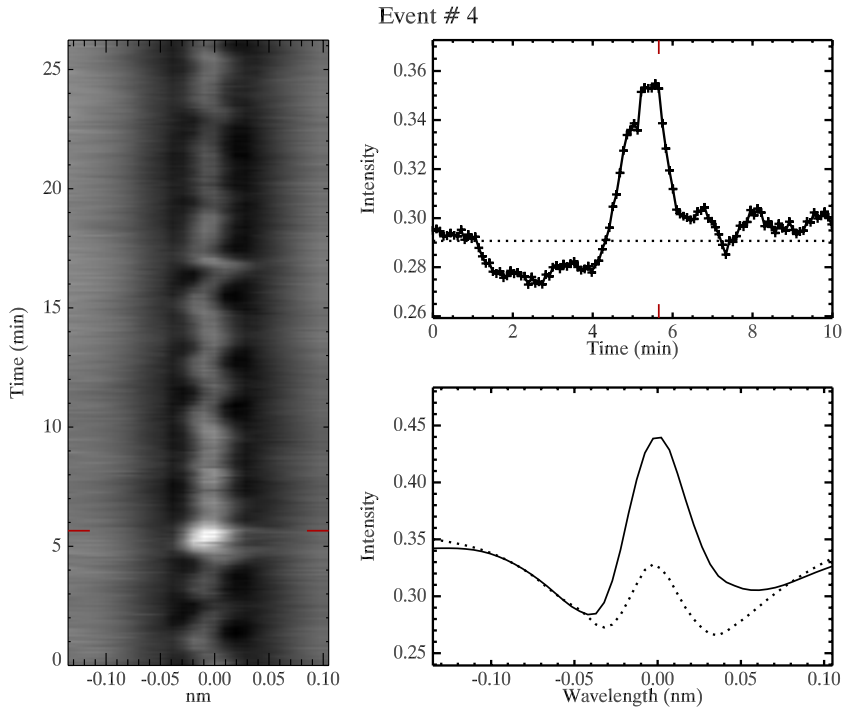

Figure 11. Spectral-temporal behavior of Event #4. Same as Figure 4.
(A color version of this figure is available in the online journal.)

The most striking feature of this event is the dramatic change in the chromospheric Ca II 854.2 nm line profile before and after the transient brightening itself, indicating a persistent modification of the chromospheric conditions following the event. In the 11 minutes prior to the brightening, the line shows a normal, nearly constant absorption profile typical of quiescent fibrils. Following the event, the line core remains filled in and brighter than at any time prior in the data set. This persistent change occurs not just at the two footpoints, but extends over the entire elongated area between the two footpoint brightenings (as can be seen in Figure 12).

Without further details on the evolution of the photospheric and chromospheric magnetic field on these small scales, or at least simultaneous measurements in other spectral lines, it is hard to infer the cause of this abrupt observed change in the spectral line profile. TRACE images in the 17.1 nm filter taken

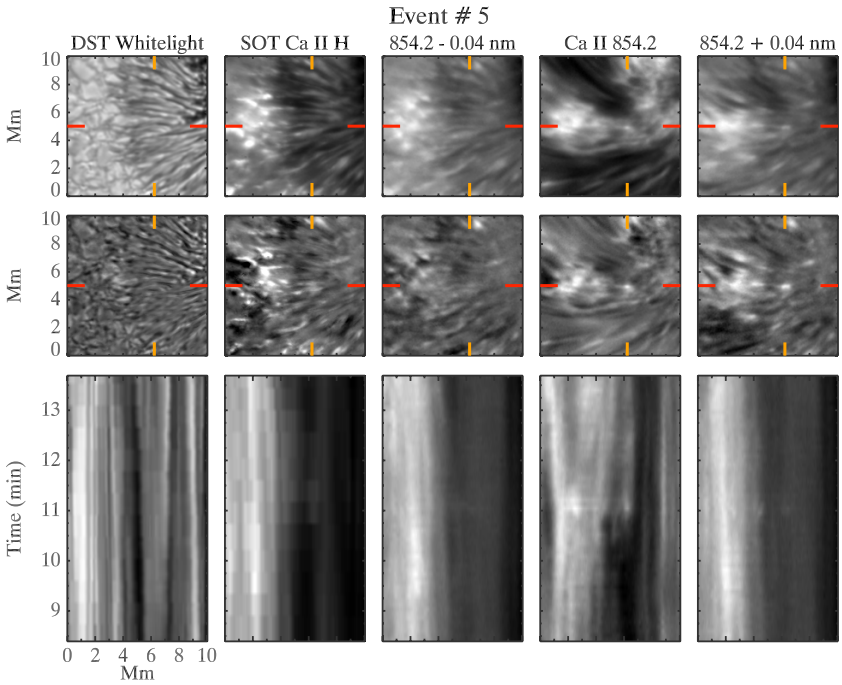

Figure 12. Spatio-temporal behavior of Event #5. Same as Figure 3.
(A color version of this figure is available in the online journal.)

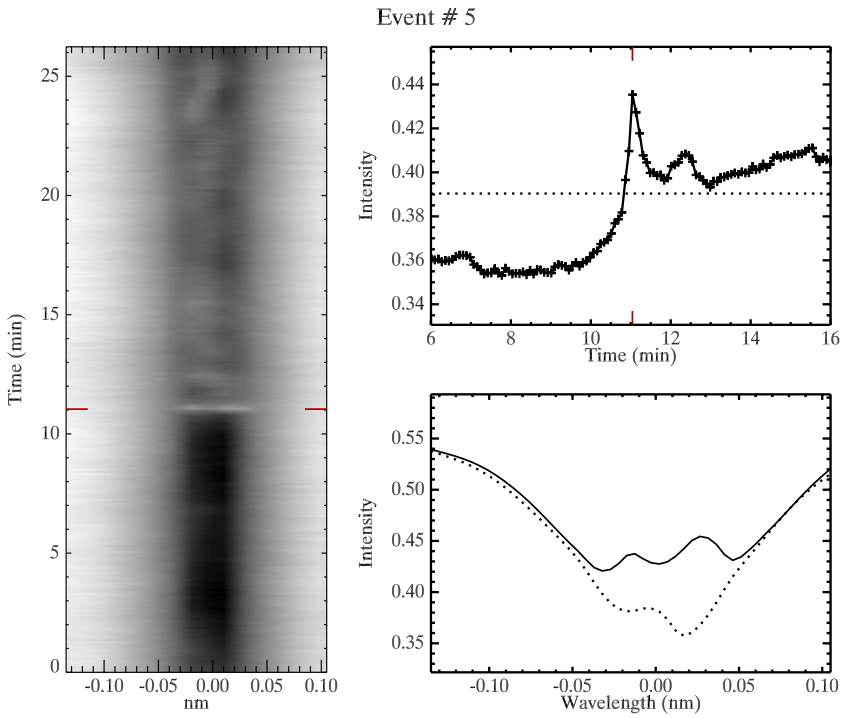

Figure 13. Spectral-temporal behavior of Event #5. Same as Figure 4.
(A color version of this figure is available in the online journal.)

during the observing sequence (but with a much slower 2-minute cadence) show no signature of a coronal response or changes in the overlying emission during this event.

One possibility is that material lying along the field lines connecting the two polarities was heated by the energy released in the reconnection event. The central intensity of the Ca II 854.2 line can be a reasonable temperature proxy, as pointed out by Cauzzi et al. (2009), consistent with such a scenario. However, this does not satisfactorily explain the consistently elevated line core brightness in the 20 minutes following the event in the absence of any other heating episodes.

Another scenario is that a small fibril was obscuring or absorbing the underlying bright, open field regions of the atmosphere. Similar line profiles, with bright line cores, are seen throughout our observing interval in this "superpenumbral gap." The material confined along the field lines at the start of

our observations was removed during the transient event through evaporation or draining (the latter perhaps more consistent with the red asymmetry of the transient profile), allowing the underlying bright regions of the atmosphere to be consistently seen.

4. CONCLUSIONS

We presented a spectroscopic study of selected transient events in the region surrounding a sunspot umbra. The events were identified in the core and wings of the Ca II 854.21 nm line observed at high spatial, spectral, and temporal resolution. We compared the appearance of these events in the spectral images with the white-light intensity and through a broadband Ca II H filter from *Hinode*. The key finding is that the observed transient brightenings show broadly similar temporal light curves in integrated intensity, but the underlying spectral profiles can be quite different.

This work was motivated by the studies of PMJs using SOT Ca II H filtergrams. Indeed, we identified several events that matched well with the identified characteristics of that phenomenon, including their lifetime and orientation with respect to the underlying penumbral fibrils. We studied two such episodes (Events #1 and #2) in detail and were able to measure the spectral behavior of these events. This showed that the enhanced emission was coming from the wings of the Ca II 854.21 profile, indicating that the energy deposition was probably occurring lower in the atmosphere, around the temperature minimum where this portion of the line profile is typically formed. The core of the Ca II 854.21 line profile was largely unchanged in these events. Similar wing emission in the Ca II H line is presumably the cause of the enhancement seen through the broad calcium filter on SOT/*Hinode*.

The enhancements confined to the wings of the line profiles are reminiscent of the spectral signature of Ellerman bombs, though the studied PMJ events are much smaller, both spatially and temporally, than canonical Ellerman bombs. However, Nelson et al. (2013) have recently studied Ellerman bombs around a sunspot in Hα at high spatial and temporal resolution and found a distribution of event sizes and lifetimes that extend down to the scale of events discussed in this paper. We found a similar spectral profile in Event #3 located in the normal granulation outside of the photospheric penumbra, indicating that such processes may occur, with reduced visibility through broader filters, even in other regions of the solar atmosphere.

One surprising finding was the presence of "precursors" to these events—a spreading enhancement seen in the wings of the line profile beginning up to 1 minute before the rapid impulsive brightening seen so clearly in the spectrally integrated line intensity. The transverse expansion of the precursor is approximately 12 km s^{-1}, relatively slow compared to the apparent expansion speeds derived from the main event brightening. The precursor may then trigger the impulsive brightening, which may subsequently show apparent expansion velocities that do not directly reflect true plasma velocities. Such behavior might be consistent with the destabilization of a complex, twisted magnetic field configuration, such as that modeled by Magara (2010). This precursor may also be consistent with the bow-shock model of Ryutova et al. (2008), in which plasma along reconnected field lines is accelerated upward by magnetic tension and buoyancy until it reaches supersonic velocities. The precursor could be the signature of the "slingshot" shock that runs out in front of the bow shock.

We also found other transients in the same sunspot that had a significantly different behavior than the PMJs. These typically showed an enhancement that extended across the entire central portion of the line profile. The duration of this increased emission was very short, scarcely resolved by the 5 s temporal cadence of our observations. These events, with their broad filling in of the line profile and impulsive light curves, are reminiscent instead of very contained flare emission, due to the magnetic reconnection in the complicated magnetic field topology of the chromosphere above the sunspot. The different "background" spectral behavior shows that the conditions may vary significantly for different regions around the sunspot. This highlights not only the significant complexity and variety of the magnetic field structure even above a rather "simple" sunspot, but also the very rapid timescales on which magnetic energy may be released in the solar atmosphere.

IBIS was constructed by INAF/OAA with contributions from the University of Florence, the University of Rome, MIUR, and MAE and is operated with support of the National Solar Observatory. The NSO is operated by the Association of Universities for Research in Astronomy, Inc., under cooperative agreement with the National Science Foundation. This research made much use of NASA's Astrophysics Data System and SolarMonitor.org.

Hinode is a Japanese mission developed and launched by ISAS/JAXA, collaborating with NAOJ as a domestic partner, NASA and STFC (UK) as international partners. Scientific operation of the *Hinode* mission is conducted by the *Hinode* science team organized at ISAS/JAXA. Support for the post-launch operation is provided by JAXA and NAOJ (Japan), STFC (U.K.), NASA, ESA, and NSC (Norway). One of the authors (Y.K.) was partially supported by the JSPS Core-to-Core Program 22001.

REFERENCES

Alissandrakis, C. E., Georgakilas, A. A., & Dialetis, D. 1992, SoPh, 138, 93
Archontis, V., & Hood, A. W. 2009, A&A, 508, 1469
Bard, S., & Carlsson, M. 2010, ApJ, 722, 888
Beckers, J. M., & Tallant, P. E. 1969, SoPh, 7, 351
Bloomfield, D. S., Lagg, A., & Solanki, S. K. 2007, ApJ, 671, 1005
Bogdan, T. J., & Judge, P. G. 2006, RSPTA, 364, 313
Canfield, R. C., Reardon, K. P., Leka, K. D., et al. 1996, ApJ, 464, 1016
Cauzzi, G., Reardon, K., Rutten, R. J., Tritschler, A., & Uitenbroek, H. 2009, A&A, 503, 577
Cauzzi, G., Reardon, K. P., Uitenbroek, H., et al. 2008, A&A, 480, 515
Cauzzi, G., Reardon, K. P., Vecchio, A., Janssen, K., & Rimmele, T. 2007, in ASP Conf. Ser. 368, The Physics of Chromospheric Plasmas, ed. P. Heinzel, I. Dorotovič, & R. J. Rutten (San Francisco, CA: ASP), 127
Cavallini, F. 2006, SoPh, 236, 415
Centeno, R., Socas-Navarro, H., Collados, M., & Trujillo Bueno, J. 2005, ApJ, 635, 670
Christopoulou, E. B., Georgakilas, A. A., & Koutchmy, S. 2000, A&A, 354, 305
Christopoulou, E. B., Georgakilas, A. A., & Koutchmy, S. 2001, A&A, 375, 617
Denker, C., de Boer, C. R., Volkmer, R., & Kneer, F. 1995, A&A, 296, 567
Ellerman, F. 1917, ApJ, 46, 298
Fang, C., Tang, Y. H., Xu, Z., Ding, M. D., & Chen, P. F. 2006, ApJ, 643, 1325
Georgakilas, A. A., Christopoulou, E. B., Skodras, A., & Koutchmy, S. 2003, A&A, 403, 1123
Georgoulis, M. K., Rust, D. M., Bernasconi, P. N., & Schmieder, B. 2002, ApJ, 575, 506
Giovanelli, R. G. 1972, SoPh, 27, 71
Hansteen, V. H., De Pontieu, B., Rouppe van der Voort, L., van Noort, M., & Carlsson, M. 2006, ApJL, 647, L73
Jurčák, J., & Katsukawa, Y. 2008, A&A, 488, L33
Jurčák, J., & Katsukawa, Y. 2010, A&A, 524, A21

Katsukawa, Y., Berger, T. E., Ichimoto, K., et al. 2007, Sci, 318, 1594
Katsukawa, Y., & Jurčák, J. 2010, A&A, 524, A20
Kitai, R., & Muller, R. 1996, SoPh, 165, 155
Kneer, F., Mattig, W., & v. Uexkuell, M. 1981, A&A, 102, 147
Kosugi, T., Matsuzaki, K., Sakao, T., et al. 2007, SoPh, 243, 3
Kurokawa, H., Kawaguchi, I., Funakoshi, Y., & Nakai, Y. 1982, SoPh, 79, 77
Magara, T. 2010, ApJL, 715, L40
Maltby, P. 1975, SoPh, 43, 91
Matsumoto, T., Kitai, R., Shibata, K., et al. 2008, PASJ, 60, 577
Neidig, D., Wiborg, P., Confer, M., et al. 1998, in ASP Conf. Ser. 140, Synoptic Solar Physics, ed. K. S. Balasubramaniam, J. Harvey, & D. Rabin (San Francisco, CA: ASP), 519
Nelson, C. J., Doyle, J. G., Erdélyi, R., et al. 2013, SoPh, 283, 307
Pariat, E., Schmieder, B., Berlicki, A., et al. 2007, A&A, 473, 279
Reardon, K. P., & Cavallini, F. 2008, A&A, 481, 897
Reardon, K. P., Uitenbroek, H., & Cauzzi, G. 2009, A&A, 500, 1239
Rimmele, T. R. 2004, Proc. SPIE, 5490, 34
Rouppe van der Voort, L. H. M., Rutten, R. J., Sütterlin, P., Sloover, P. J., & Krijger, J. M. 2003, A&A, 403, 277
Roy, J.-R., & Leparskas, H. 1973, SoPh, 30, 449
Ryutova, M., Berger, T., & Title, A. 2008, ApJ, 676, 1356
Sakai, J. I., & Smith, P. D. 2008, ApJL, 687, L127
Scherrer, P. H., Bogart, R. S., Bush, R. I., et al. 1995, SoPh, 162, 129
Schmieder, B., & Pariat, E. 2007, SchpJ, 2, 4335
Schmieder, B., Pariat, E., Aulanier, G., et al. 2002, in Solar Variability: From Core to Outer Frontiers, ed. A. Wilson (ESA SP-506; Noordwijk: ESA), 911
Severny, A. B. 1956, Obs, 76, 241
Socas-Navarro, H., McIntosh, S. W., Centeno, R., de Wijn, A. G., & Lites, B. W. 2009, ApJ, 696, 1683
Socas-Navarro, H., Pillet, V. M., Elmore, D., et al. 2006, SoPh, 235, 75
Socas-Navarro, H., Trujillo Bueno, J., & Ruiz Cobo, B. 2000, Sci, 288, 1396
Stangalini, M., Del Moro, D., Berrilli, F., & Jefferies, S. M. 2011, A&A, 534, A65
Tsuneta, S., Ichimoto, K., Katsukawa, Y., et al. 2008, SoPh, 249, 167
Vecchio, A., Cauzzi, G., & Reardon, K. P. 2009, A&A, 494, 269
Vecchio, A., Cauzzi, G., Reardon, K. P., Janssen, K., & Rimmele, T. 2007, A&A, 461, L1
Watanabe, H., Vissers, G., Kitai, R., Rouppe van der Voort, L., & Rutten, R. J. 2011, ApJ, 736, 71
Wöger, F., & von der Lühe, O. 2007, ApOpt, 46, 8015
Zirin, H., & Stein, A. 1972, ApJL, 178, L85